

# A Microfluidic Study of Megakaryocytes Membrane Transport Properties to Water and Dimethyl Sulfoxide at Suprazero and Subzero Temperatures

Hsiu-Yang Tseng,<sup>1</sup> Sijie Sun,<sup>2</sup> Zhiquan Shu,<sup>1</sup> Weiping Ding,<sup>1</sup> Jo-Anna Reems,<sup>3,4</sup> and Dayong Gao<sup>1,2</sup>

Megakaryocytes (MKs) are the precursor cells of platelets. Cryopreservation of MKs is critical for facilitating research investigations about the biology of this important cell and may help for scaling-up *ex-vivo* production of platelets from MKs for clinical transfusion. Determining membrane transport properties of MKs to water and cryoprotectant agents (CPAs) is essential for developing optimal conditions for cryopreserving MKs. To obtain these unknown parameters, membrane transport properties of the human UT-7/TPO megakaryocytic cell line were investigated using a microfluidic perfusion system. UT-7/TPO cells were immobilized in a microfluidic system on poly-D-lysine-coated glass substrate and perfused with various hyper-osmotic salt and CPA solutions at suprazero and subzero temperatures. The kinetics of cell volume changes under various extracellular conditions were monitored by a video camera and the information was processed and analyzed using the Kedem–Katchalsky model to determine the membrane transport properties. The osmotically inactive cell volume ( $V_b=0.15$ ), the permeability coefficient to water ( $Lp$ ) at 37°C, 22°C, 12°C, 0°C, -5°C, -10°C, and -20°C, and dimethyl sulfoxide (DMSO;  $Ps$ ) at 22, 12, 0, -10, -20, as well as associated activation energies of water and DMSO at different temperature regions were obtained. We found that MKs have relatively higher membrane permeability to water ( $Lp=2.62\ \mu\text{m}/\text{min}/\text{atm}$  at 22°C) and DMSO ( $Ps=1.8\times 10^{-3}\ \text{cm}/\text{min}$  at 22°C) than most other common mammalian cell types, such as lymphocytes ( $Lp=0.46\ \mu\text{m}/\text{min}/\text{atm}$  at 25°C). This information could suggest a higher optimal cooling rate for MKs cryopreservation. The discontinuity effect was also found on activation energy at 0°C–12°C in the Arrhenius plots of membrane permeability by evaluating the slope of linear regression at each temperature region. This phenomenon may imply the occurrence of cell membrane lipid phase transition.

## Introduction

PLATELET TRANSFUSIONS ARE a highly effective for treating bleeding disorders in patients with low platelet counts and/or functionally defective platelets. Currently, around 10.3 million units of platelets are transfused in the United States annually.<sup>1</sup> Since platelets can only be stored at room temperature for 5 days,<sup>2</sup> this coupled with the demand for platelets can result in shortages of transfusable platelets.

Megakaryocytes (MKs), which are produced from hematopoietic stem cells (HSCs), are giant cells capable of producing around  $10^4$  platelets.<sup>2,3</sup> To produce platelets, MKs undergo a cytoplasmic maturation that involves the formation of proplatelet processes that extend into marrow sinusoids, where shear forces generated from blood flow facilitate the release of the proplatelet processes.<sup>4,5</sup>

Understanding the molecular pathways and physical mechanisms *in vivo* and *in vitro* that regulate MK develop-

ment and platelet release are of significant interest by the hematology field.<sup>6,7</sup> *Ex vivo* large-scale generation of platelets from MKs is also emerging as a possible solution to platelet shortages.<sup>8–10</sup> However, MKs constitute only 0.03%–0.06% of all nucleated cells in the bone marrow and are difficult to isolate in large numbers<sup>11</sup>; further, the generation and amplification of MKs from HSCs is time consuming and costly, and can take >10 days.<sup>12</sup> Therefore, the ability to cryopreserve MKs after HSCs differentiation and before platelet production could provide crucial flexibility in producing platelets *in vitro* on a large scale.

To successfully achieve cryopreservation, one has to prevent possible cryoinjury to the cells, which is most likely to occur at a temperature around -20°C during the freezing and thawing processes. This is a temperature where extracellular ice formation and the rising of solute concentration in the surroundings may induce intracellular ice formation (IIF)<sup>13,14</sup> and excessive volume shrinkage<sup>15,16</sup> when the

<sup>1</sup>Departments of Mechanical Engineering, <sup>2</sup>Bioengineering, and <sup>3</sup>Hematology, University of Washington, Seattle, Washington.  
<sup>4</sup>Puget Sound Blood Center, Seattle, Washington.

cooling rate is too high and low, respectively.<sup>17</sup> To develop optimized protocols for freezing, thawing, and removal of cryoprotectant agent (CPA) for different cell types, the cell membrane transport properties at subzero temperatures need to be determined. Specifically, these properties are the membrane permeability coefficient to water ( $Lp$ ), the membrane permeability coefficient to CPAs ( $Ps$ ), and the activation energies of all permeability coefficients ( $Ea$ ). Currently, the membrane transport properties of human MKs have not been determined yet.

In previous works, we proposed that cell membrane permeability could be determined by several techniques by measuring cell volume change under controlled anisotonic conditions, such as microdiffusion,<sup>18</sup> micropipette perfusion,<sup>19,20</sup> microperfusion chamber,<sup>21</sup> and differential scanning calorimetry (DSC).<sup>22,23</sup> However, there were difficulties associated with each of these techniques. The dialysis membrane method sometimes introduced complicated mass transfer and concentration gradient with the membrane,<sup>18</sup> and the micropipette method can only hold a single or a few cells in one experiment and is limited to cell types with large size and shell.<sup>19,20</sup> The microperfusion chamber provides an improved microfluidic tool<sup>21</sup>; however, nonuniform flow and induced cell deformation due to its cell blocking geometry may also generate a heterogeneous exchange rate of mass between intra- and extraenvironment. Importantly, very few such data from above direct-observation methods at subzero temperatures are reported. Toner et al. have measured volumes of embryos between 0°C and -20°C at a low cooling rate (-2°C/min) with direct cryomicroscope observations,<sup>13</sup> but in our study this method was found to provide inaccurate membrane transport information for MKs as a large cell type due to the presence and growth of extracellular ice, which may squeeze and damage the cell membrane integrity during freezing. The presence of the extracellular ice also makes the image processing for measuring the cell volume difficult. The DSC has been used to derive water permeability and activation energy of mammalian sperm by measuring latent heat change during freezing at subzero temperatures.<sup>22</sup> However, the difference of the latent heat curve may not be distinguishable for cell types with high permeability that require a high cooling rate to induce IIF.<sup>23</sup> Limited ability on measuring membrane permeability to CPAs and the cost of the DSC also make the popular use of this method difficult.

To overcome above-mentioned difficulties and achieve membrane transport properties measurement at subzero temperatures under a light microscope, we developed a simple cell-adhesive microperfusion system that could replace isotonic medium in the channel with desired solutions in less than a second. Besides, for a microscale problem, diffusion at the boundary between 2 consecutive solutions is negligible. Rapid heat transfer and uniform temperature distribution was ensured due to low heat capacity of solutions in the microfluidic channel. It is also observed that fluids in this microenvironment easily remain supercooled at temperatures below the freezing point.<sup>24</sup> Hydrophobic surfaces of the polydimethylsiloxane (PDMS) microchannel further facilitated supercooling of solutions at subzero temperatures.<sup>25</sup> Our microperfusion channel maintained the isotonic solution ice-free down to around -23°C. This new system was applied to determining the membrane transport properties of MKs.

## Materials and Methods

### Theory of cell membrane transport model

*Evaluation of water permeability.* The semi-permeable feature of the cell membrane regulates the water and solute transport between intracellular and extracellular environments. Osmotic pressure gradient across the plasma membrane produces cell volume changes until reaching equilibrium. The intracellular osmolality during hypertonic shrinkage can be described by the Boyle van't-Hoff relationship:<sup>26</sup>

$$C_i = C_0 \cdot \left( \frac{V_0 - V_b}{V - V_b} \right) \quad (1)$$

where  $C_i$  is intracellular osmolality,  $C_0$  is the isotonic osmolality in cells,  $V$  is the cell volume,  $V_0$  is the isotonic cell volume, and  $V_b$  is the osmotically inactive volume in cells.

The osmotically inactive fraction,  $V_b$ , can be determined by the Boyle van't-Hoff plot. Graphing the cell's osmotic equilibrium volume in solutions with different salt concentrations results in a line with an intercept of the  $y$ -axis that is the osmotically inactive fraction of the cell type being evaluated.

The kinetic of the cell volume change as a function of time induced by water flux across the plasma membrane is given by the following equation:<sup>18-21</sup>

$$\frac{dV}{dt} = Lp \cdot A \cdot R \cdot T \cdot (C_i - C_e) \quad (2)$$

where  $Lp$  is water permeability coefficient,  $A$  is the surface area of the membrane,  $R$  is the ideal gas constant, and  $T$  is the temperature. The  $Lp$  values of cells at different temperatures can be determined by least-square curve fitting after cells were perfused by desired hypertonic solutions.<sup>19-21</sup>

Water permeability coefficients for the same cell type can also vary dramatically with temperature.<sup>27</sup> Membrane permeability's dependency on temperature can be described by the Arrhenius relation:<sup>28,29</sup>

$$Lp(T) = Lp_{,ref} \cdot \exp \left[ \frac{-Ea}{R} \cdot \left( \frac{1}{T} - \frac{1}{T_{ref}} \right) \right] \quad (3)$$

where  $Lp_{,ref}$  is the water membrane permeability coefficient at a known temperature ( $T_{ref}$ ),  $Ea$  is the activation energy, and  $R$  is the universal gas constant.

Taking the natural logarithm, equation 3 is rearranged to be

$$\ln(Lp(T)) = - \frac{Ea}{R \cdot T} + Constant \quad (4)$$

*CPA transport through cell membrane.* During cryopreservation, the transport of water and solutes across cell membrane both take place and interact with each other when a permeating CPA is used. To describe the cell volume kinetic when there is a ternary system (water, permeable CPA, and impermeable salts), the 2-parameter model is used:<sup>30,31</sup>

$$\frac{dV}{dt} = \frac{dV_{water}}{dt} + \frac{dV_{CPA}}{dt} \quad (5)$$

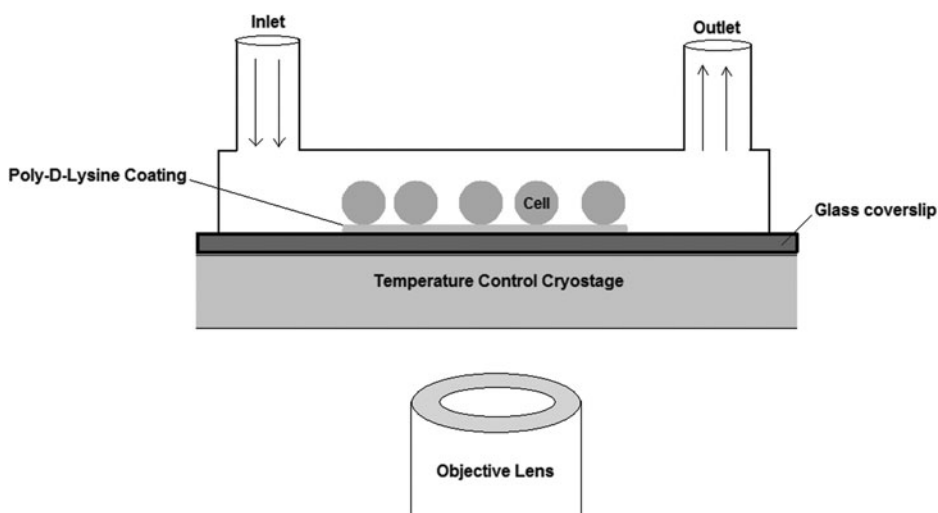


**FIG. 1.** Schematic diagram showing the orientation of a microperfusion system positioned on a temperature-controlled cryostage relative to an objective lens of an inverted microscope. Also shown are cells adhering to a poly-D-Lysine-coated slide within a microperfusion channel with inlet and outlet ports.

where

$$\begin{aligned} \frac{dV_{water}}{dt} &= Lp \cdot A \cdot R \cdot T \cdot (C_i - C_e) \\ \frac{dV_{CPA}}{dt} &= Ps \cdot A \cdot (C_{e,CPA} - C_{i,CPA}) \cdot \bar{V}_{CPA} \end{aligned} \quad (6)$$

where  $C_i$  and  $C_e$  are total solutes osmolality (eg, CPA and salts) in and out of the cell, respectively,  $Ps$  is the permeability coefficient to the CPA,  $C_{e,CPA}$ , and  $C_{i,CPA}$  are CPA osmolality in and out of the cell, respectively,  $\bar{V}_{CPA}$  is the partial molar volume of the CPA. The  $Lp$  and  $Ps$  values can be determined by least square curve fitting after cells were perfused by desired CPA solutions.<sup>19–21</sup>

### Source and preparation of cells

In this study, a human megakaryocytic cell line (UT-7/TPO) was used as a model cell type to investigate membrane properties of human MKs when cryopreserved in the presence of water and dimethyl sulfoxide (DMSO) at suprazero and subzero temperatures. UT-7/TPO, a suspension cultured cell line, was established from the bone marrow of a patient with acute megakaryocytic leukemia.<sup>32</sup> The diameter of the cell is approximately 5–20  $\mu\text{m}$  at early stages of development with well-rounded spherical shape, and can mature to become a cell of approximately 70  $\mu\text{m}$  when cultured with a Src kinase inhibitor, SU6656.<sup>24</sup> UT-7/TPO cells can be absolutely stimulated and controlled to express very similar biophysical features to human MKs in bone marrow.<sup>11,33,34</sup>

These cells were cultured using Isocove's modified Dulbecco's medium (Gibco) with 10% fetal bovine serum, 1 mM Glutamine (Gibco) 1  $\times$  Penicillin (Gibco), Streptomycin (Gibco), and 10 ng/mL recombinant human thrombopoietin (TPO; Peprotech). UT-7/TPO cells were maintained in sterilized Petri plates or T-25 flasks at 37°C in a humidified atmosphere containing 5%  $\text{CO}_2$ . Cultured cells were prepared for testing by centrifuging them at 1500 rpm for 5 min, washing with 1  $\times$  phosphate-buffered saline (PBS), and resuspending the cells in culture medium with osmolality of 273 mosm/kg. Manual cells counts were performed using a light microscope and hemacytometer (Hausser Scientific). Cell suspensions with average cell densities of approximately  $1 \times 10^6$  cells/mL were used within 12 h.

### Design and fabrication of the surface-treated microperfusion channel

Microperfusion channels were designed to measure cell volume changes at subzero temperatures. The size of the microchannel was small enough to ensure stable supercooling and large enough to allow cells to flow through the channel. As shown in Fig. 1, cells were immobilized onto glass slides treated with Poly-D-lysine Hydrobromide (P1149, Sigma-Aldrich) diluted to the concentration of 50  $\mu\text{g}/\text{mL}$ . The microchannel was fabricated by standard soft lithographic rapid prototyping and replica molding with PDMS (Sylgard 184, Dow-Corning Corp.). The PDMS rectangular microchannel with dimensions of 200  $\mu\text{m} \times 200 \mu\text{m} \times 2 \text{ cm}$

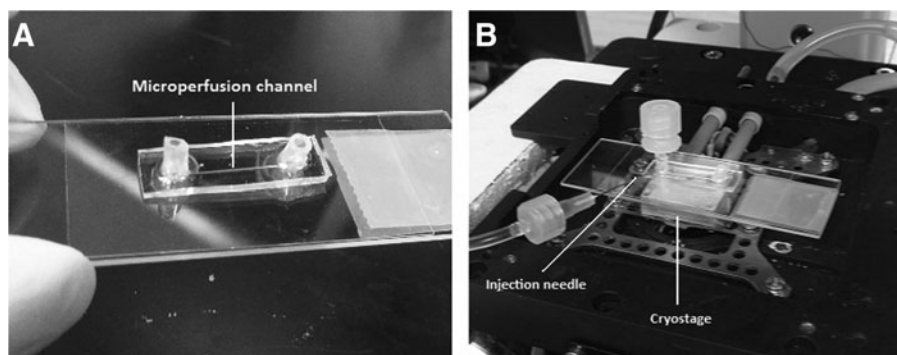
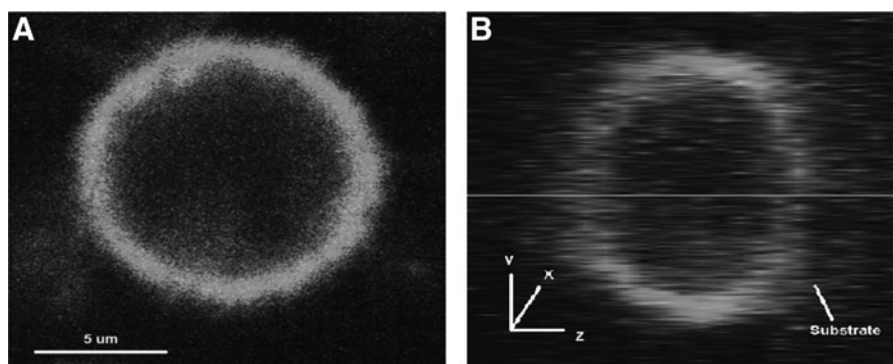


**FIG. 2.** The microperfusion system. (A) PDMS microperfusion channel situated on poly-D-lysine-coated slide (ie, microperfusion system). Arrow points to microperfusion channel. (B) The microperfusion system is located on a temperature-controlled cryostage. Arrow points to injection needle attached to tubing extending from an adapter on the inlet port. PDMS, polydimethylsiloxane.

**FIG. 3.** Confocal images of a UT-7/TPO cell stained with a membrane dye, MINI67, that are immobilized on a poly-D-lysine-coated glass coverslip. **(A)** Top view ( $x$ - $y$  plane). **(B)** Right side view ( $y$ - $z$  plane).



was placed and pressed carefully onto the surface-treated glass slide.

The microperfusion chamber was placed on the top of a cryostage (HSC601, Instec Inc., Boulder, CO) connected to a liquid nitrogen pump and a controller (STC200, Instec Inc.). The cryostage system was monitored and operated using Wintemp software. The cryostage can reach temperatures ranging from  $-150^{\circ}\text{C}$  to  $500^{\circ}\text{C}$ , which satisfied our desired temperature range of  $37^{\circ}\text{C}$  to approximately  $-20^{\circ}\text{C}$ . UT-7/TPO cells immobilized in the microperfusion system were visualized with an inverted microscope (TE2000-S, Nikon) and imaged with a CMOS high speed camera (Hot Shot 1280, Nac Technology).

#### Manipulation of the experiments

The microperfusion channel was placed and secured with an adhesive sticker to the top of the temperature-controlled cryostage as shown in Fig. 2. Temperatures were set to be  $37^{\circ}\text{C}$ ,  $22^{\circ}\text{C}$ ,  $12^{\circ}\text{C}$ ,  $0^{\circ}\text{C}$ ,  $-5^{\circ}\text{C}$ ,  $-10^{\circ}\text{C}$ , and  $-20^{\circ}\text{C}$ . The whole system was observed by using an inverted microscope and recorded by the CMOS camera. About  $10\ \mu\text{L}$  cell suspensions at a density of approximately  $10^5$  cells/mL were injected into the channel from the inlet. This procedure was done carefully to avoid any air bubbles that are highly damaging to cells. Cells were allowed to adhere to the substrate for 1 min and a viewing region with the most cells was chosen for imaging. Tubing was attached to the inlet port so that hypertonic solutions with different concentrations of salts ( $2\times$  and  $3\times$  PBS) and CPA ( $10\%$  DMSO +  $10\%$   $10\times$  PBS + water) could be injected into the inlet tube using a needle connected to a 10 mL syringe mounted on a syringe pump (Aladdin-IM, World Precision Instrument; Fig. 2). The solution replacement time can cause errors when calculating membrane permeability, yet it can be reduced if perfusion speed is increased. To minimize inconsistency and error between the real experiment and theoretical assumption, in our experiment, the perfusion flow speed was increased to  $36\ \mu\text{L}/\text{min}$  ( $600\ \text{nL}/\text{s}$ ) along the main microchannel ensuring  $<0.4\ \text{s}$  replacement time. All solutions were passed through a  $0.2\ \mu\text{m}$  syringe filter to preclude large impurities that could be ice nucleation sites at low temperatures. Immobilized cells were monitored at a speed of 60 frames per second for 46 s. For low temperature experiments, a droplet of propylene glycol (CQ Concept Inc.) was placed on top of the PDMS microchannel to avoid water vapor condensation. To minimize possible errors from temperature measurement, we waited for few minutes before the experiment started so that we were sure the whole microfluidic device

already reached the desired temperature. Besides, preliminary tests were done by inserting a K-type thermocouple (SA-1K, Omega) into the PDMS device very close to the microchannel during fabrication, indicating that the temperature near the microchannel was consistent to the set temperature.

The confocal microscope (Zeiss LSM510 Confocal Microscope, Zeiss) was employed to visualize the 3D shape of immobilized cells attached to substrate to determine the condition of inactive surface area of membrane for our design. Cell membranes were stained with green fluorescence (MINI67, Sigma-Aldrich) and excited by blue light ( $\lambda = 498\ \text{nm}$ ). The experiment took place at the Nanotechnology Center (University of Washington, Seattle).

## Results

### Inactive surface area of the cell membrane on the substrate

When calculating the membrane transport properties ( $L_p$  and  $P_s$ ), the surface area of the plasma membrane is one of the variables in equations 2 and 6. In previous work from others,<sup>20,21</sup> the membrane surface area of a spherical cell was assumed to be freely open and fully considered, even though there must be some inactive area for mass transfer between cytoplasm and extracellular medium due to contact with device geometry and deformation. Immobilized UT-7/TPO cells on the substrate of the microperfusion channel were stained and imaged by using the confocal microscope. In

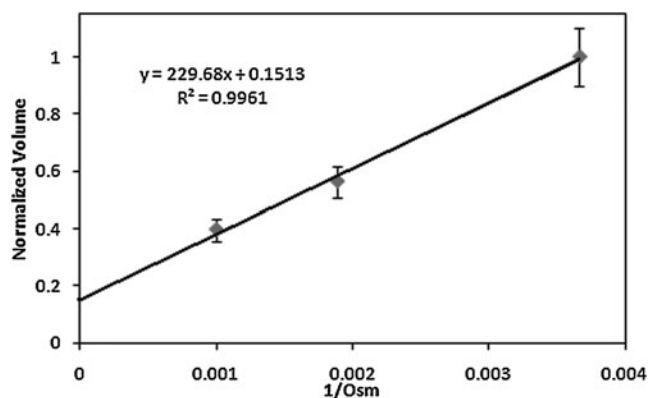


**FIG. 4.** Boyle Van't-Hoff relationships for UT-7/TPO cells at  $37^{\circ}\text{C}$ . The osmotically inactive cell volume ( $V_b$ ) is determined to be 0.15 of initial volume.

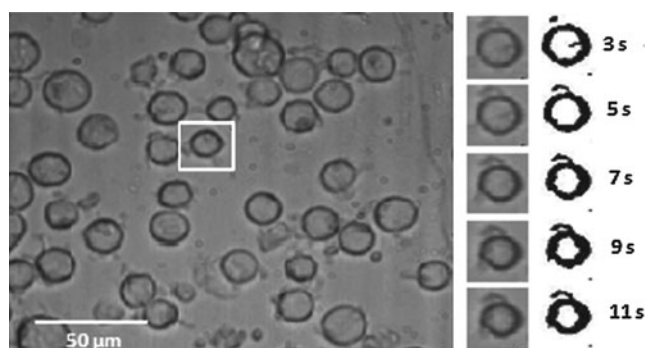


FIG. 5. (Left) UT-7/TPO cells immobilized on surface-treated substrate in a microchannel perfused with  $3\times$  PBS. (Right) Grayscale and binary images of the single cell in the cropped area (rectangle) at each time slide. PBS, phosphate-buffered saline.

Fig. 3, the z-direction of the cell image shows surface adhesion to the substrate. The flat shape of the cell was due to gravity. The cell image was analyzed using ImageJ (National Institutes of Health) to obtain an average value of  $A_{inactive}$  of approximately 0.17 of initial cell membrane surface area ( $\pm 0.05$ ,  $n=9$ ). This portion of surface area is subtracted from each measurement.

#### Determination of $V_b$ , $L_p$ , $P_s$ , and $E_a$

Osmotically inactive cell volume,  $V_b$ , can be calculated through the Boyle van't-Hoff plot shown in Fig. 4. The equilibrium cell volume in  $1\times$ ,  $2\times$ , and  $3\times$  PBS solution were averaged and the linear regression estimated  $V_b$  to be 0.15 ( $n=10$ ,  $r^2=0.996$ ) of the normalized cell volume.

The cell volume change with respect to time and intracellular/extracellular solute concentrations were obtained directly from analyzing the image sequence of cells. Images of different time slices are shown in Fig. 5 and illustrate shrinkage of the cell volume during hypertonic perfusion. The cell images at each time frame were converted to be binary at a set threshold to sharpen the cell outlines. Cell volumes were measured by counting the number of pixels in cells with MATLAB image processing (Mathworks, Inc.). The normalized cell volume curve as shown in Figs. 6 and

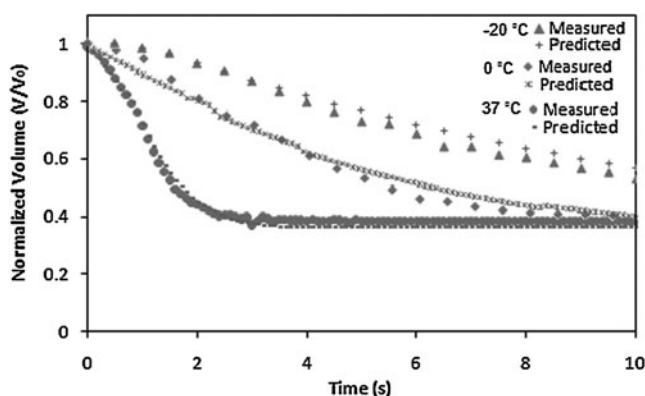


FIG. 6. Normalized cell volume change with respect to time when cells are perfused with  $3\times$  PBS at  $-20^\circ\text{C}$ ,  $0^\circ\text{C}$ , and  $37^\circ\text{C}$ .

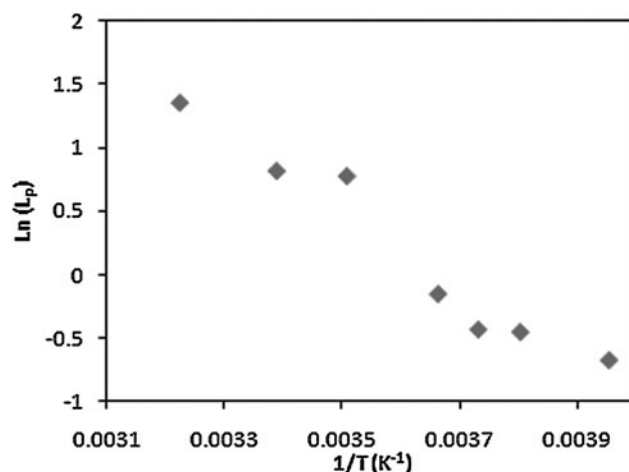


FIG. 7. Arrhenius plot of the UT-7/TPO cells showing the natural logarithms of the average water membrane permeability coefficient ( $L_p$ ) versus the reciprocal of the absolute temperatures.

8 was then analyzed by least-square curve-fitting tool provided by MATLAB to derive  $L_p$  and  $P_s$  values at different suprazero and subzero temperatures. The listed values in Tables 1 and 2 were validated through testing with a simulation to predict cell volume curves in Figs. 6 and 8, showing that UT-7/TPO cells attain cell volume equilibrium when perfused with  $3\times$  PBS at  $37^\circ\text{C}$  within 5 s. The result indicates that MKs have relatively higher membrane permeability ( $L_p=2.62\ \mu\text{m}/\text{min}/\text{atm}$  at  $22^\circ\text{C}$ ) than most other common mammalian cell types, such as lymphocytes ( $L_p=0.46\ \mu\text{m}/\text{min}/\text{atm}$  at  $25^\circ\text{C}$ ),<sup>35</sup> rat basophilic leukemia ( $L_p=0.32\ \mu\text{m}/\text{min}/\text{atm}$  at  $22^\circ\text{C}$ ),<sup>21</sup> and human umbilical cord blood CD34+ cells ( $L_p=0.17\ \mu\text{m}/\text{min}/\text{atm}$  at  $22^\circ\text{C}$ ),<sup>36</sup> which require  $>20$  s to attain cell volume equilibrium under the same perfusion condition.

The temperature dependency of the UT-7/TPO cells membrane permeability is described by the Arrhenius plot shown in Figs. 7 and 9, where the activation energy of the cell membrane for water and DMSO are derived by estimating the slope of the linear regression line at each

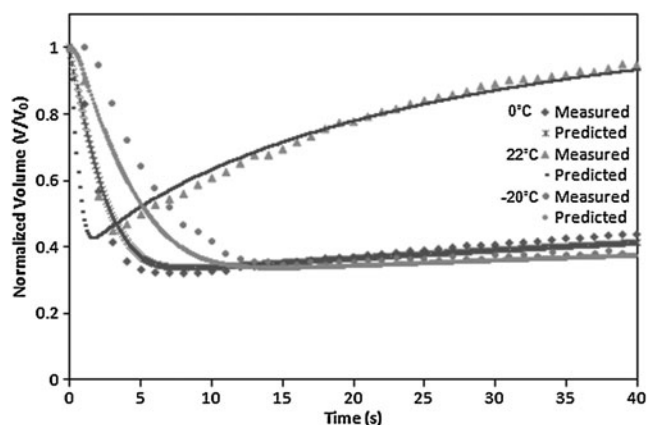


FIG. 8. Normalized cell volume change with respect to time when cells are perfused with 10% DMSO + 0.9% NaCl at  $0^\circ\text{C}$ ,  $22^\circ\text{C}$ , and  $-20^\circ\text{C}$ . DMSO, dimethyl sulfoxide.

TABLE 1. WATER PERMEABILITY COEFFICIENTS FOR UT-7/TPO CELLULAR MEMBRANES

Temperature (°C)	$L_p$ ( $\mu\text{m}/\text{min}/\text{atm}$ ) mean $\pm$ SD (n, $r^2$ )
37	$3.87 \pm 0.39$ (9, 0.85)
22	$2.26 \pm 0.11$ (8, 0.87)
12	$2.17 \pm 0.04$ (8, 0.82)
0	$0.86 \pm 0.20$ (10, 0.91)
-5	$0.65 \pm 0.06$ (9, 0.88)
-10	$0.62 \pm 0.02$ (9, 0.93)
-20	$0.51 \pm 0.07$ (10, 0.84)

Mean values from at least 3 experiments.  
SD, standard deviation.

temperature region. The activation energy values are listed in Table 3, showing that  $E_a$  values vary at different temperature regions.

## Discussion

In this study the membrane transport properties,  $V_b$ ,  $L_p$ ,  $P_s$ , and  $E_a$ , of UT-7/TPO cells were measured by using a microperfusion system and determined by analyzing the cell volume kinetics recorded from the experiments. The results in Tables 1 and 2 indicate that MKs have relatively higher membrane permeability to water and DMSO than most other common mammalian cell types, such as lymphocytes etc, indicating that the cell volume of the UT-7/TPO cell would shrink fast during the freezing process, and conceptually suggesting a high optimal cooling rate for cryopreserving MKs to avoid excessive cell shrinkage.

Intuitively, temperature dependency of the membrane permeability would diminish the fluid movement across the cell membrane when lowering temperature. The cell volume curves at high temperatures show that the cells shrank much more rapidly to the equilibrium volume within few seconds after starting perfusion in  $3 \times$  PBS solution, whereas the volume shrinkage reacted comparatively slower at subzero temperatures. We also noticed that the linear tendency of cell membrane permeability coefficients throughout the temperature range has a discontinuous phenomenon around  $12^\circ\text{C}$ – $0^\circ\text{C}$ . The phenomenon is much more obvious for cell membrane permeability to DMSO than water as shown in Table 3. The discontinuity implies that the cell membrane might own distinct activation energies at different temperatures for some unknown reasons.

TABLE 2. DIMETHYL SULFOXIDE PERMEABILITY COEFFICIENTS FOR UT-7/TPO CELLS

Temperature (°C) (n, $r^2$ )	$P_s$ ( $10^{-3}$ cm/min) mean $\pm$ SD	$L_p$ ( $\mu\text{m}/\text{min}/\text{atm}$ ) mean $\pm$ SD
22 (10, 0.70)	$1.8 \pm 0.1$	$2.5 \pm 0.15$
12 (9, 0.68)	$1.32 \pm 0.05$	$1.9 \pm 0.06$
0 (10, 0.71)	$0.13 \pm 0.011$	$0.7 \pm 0.01$
-10 (9, 0.69)	$0.09 \pm 0.02$	$0.60 \pm 0.03$
-20 (9, 0.73)	$0.06 \pm 0.03$	$0.58 \pm 0.015$

Mean values from at least 3 experiments.

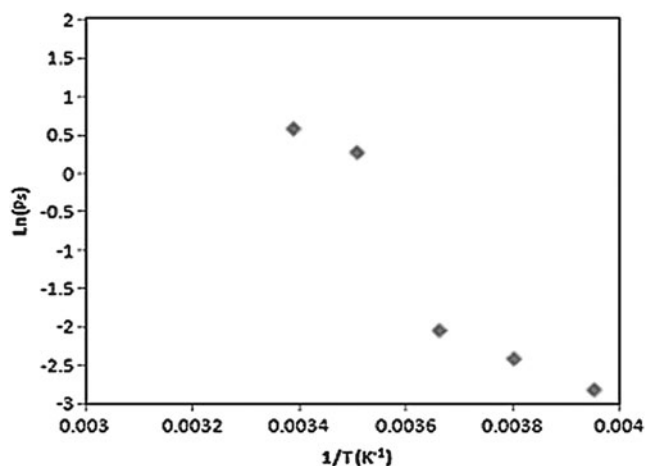


FIG. 9. Arrhenius plot of the UT-7/TPO cells showing the natural logarithms of the average DMSO membrane permeability coefficient ( $P_s$ ) versus the reciprocal of the absolute temperature.

It was found that the activation energy of the membrane could vary at different temperature ranges.<sup>37,38</sup> Noiles et al. have also reported this temperature dependence in water membrane permeability of the mouse sperm plasma membrane showing a discontinuity between  $4^\circ\text{C}$  and  $0^\circ\text{C}$ .<sup>38</sup> Our investigation extended the membrane permeability measurement to lower temperatures revealing that  $E_a$  seems to increase at  $12^\circ\text{C}$ – $0^\circ\text{C}$ , whereas  $E_a$  values are relatively similar for high ( $12^\circ\text{C}$ – $37^\circ\text{C}$ ) and low ( $0^\circ\text{C}$ – $20^\circ\text{C}$ ) temperature ranges. The variation of activation energy at different temperatures might be associated with the lipid phase transition of the cell membrane, where the plasma membrane could possibly experience lipid phase transition during cooling caused from several possible factors, including liquid–gel (solid) phase change of lipid and membrane protein conformational change.<sup>39–42</sup>

In this study, the cell-adhesive microperfusion system was successfully implemented to visualize MK cell volume change in hypertonic solutions and DMSO solutions. The membrane permeability coefficients and activation energy of MKs for water and DMSO were measured at suprazero and subzero temperatures, which are critical information for optimal cryopreservation of MKs. The cell adhesive method in the microperfusion system may also be developed in the future to study biomechanical influences of the extracellular environment on other MKs functions, such as proplatelet

TABLE 3. ACTIVATION ENERGY OF UT-7/TPO CELLS FOR WATER AND DIMETHYL SULFOXIDE

Temperature (°C)	$E_a$ water (Kcal/mol) ( $r^2$ )	$E_a$ DMSO (Kcal/mol) ( $r^2$ )
37 to 12	2.12 (0.87)	2.53 (0.99)
12 to 0	6.00 (1)	15.0 (1)
0 to 20	1.63 (0.89)	2.67 (1)
37 to -20	3.06 (0.94)	6.03 (0.91)

Mean values from at least 3 experiments.  
DMSO, dimethyl sulfoxide.

formation. In conclusion, the presented study allows us to immobilize a monolayer of cells on a substrate with a simple and convenient approach, and it provides us an extended insight on the membrane transport properties for a wide range of temperature.

### Acknowledgments

This work was supported by a grant from NIH and FHCRC. The authors thank Mr. Yuan-Lung Luo in the UW Physics Department and Mr. Tim Chang in the UW Bioengineering Department for suggestions and deep discussions.

### Author Disclosure Statement

No competing financial interests exist.

### References

- Battinelli E, Hartwig J, Italiano J. Delivering new insight into the biology of megakaryopoiesis and thrombopoiesis. *Curr Opin Hematol* 2007;14:419–26.
- Wolkersa W, Walker N, Tablin F, et al. Human platelets loaded with trehalose survive freeze-drying. *Cryobiology* 2002;42:79–87.
- Chang Y, Bluteau D, Debili N, et al. From hematopoietic stem cells to platelets. *J Thromb Haemost* 2007;5:318–327.
- Geddis A. The regulation of proplatelet formation. *Haematologica* 2009;94:756–759.
- Junt T, Schulze H, Chen Z. Dynamic visualization of thrombopoiesis within bone marrow. *Science* 2007;317:1767–1770.
- Tablin F, Castro M. Blood platelet formation *in vitro*. The role of the cytoskeleton in megakaryocyte fragmentation. *J Cell Sci* 1990;97:59–70.
- Sabri S, Jandrot-Perrus M, Bertoglio J, et al. Differential regulation of actin stress fiber assembly and proplatelet formation by  $\alpha_2$  integrin and GPIIb/IIIa in human megakaryocytes. *Blood* 2004;104:3117–3125.
- Matsunaga T, Tanaka I, Kobune M, et al. *Ex vivo* large-scale generation of human platelets from cord blood CD34+ cells. *Stem Cells* 2006;24:2877–2887.
- Fujimoto T, Kohata S, Suzuki H, et al. Production of functional platelets by differentiated embryonic stem (ES) cells *in vitro*. *Blood* 2003;102:4044–4051.
- Sullenbarger B, Bahng H, Gruner R, et al. Prolonged continuous *in vitro* human platelet production using three dimensional scaffolds. *Exp Hematol* 2009;37:101–110.
- Komatsu N. Culture of megakaryocytic cell lines. In Gibbins JM, Mahaut-Smith MP, eds. *Platelets and Megakaryocytes*. Totowa, NJ: Humana Press Inc;2004:361–367.
- Zweegman S, van den Born J, Mus A, et al. Bone marrow stromal proteoglycans regulate megakaryocytic differentiation of human progenitor cells. *Exp Cell Res* 2004;299:383–92.
- Toner M, Cravalho E, Stachecki J, et al. Nonequilibrium freezing of one-cell mouse embryos membrane integrity and development potential. *Biophys J* 1993;64:1908–1921.
- Mazur P. Freezing of living cells—mechanisms and implications. *Am J Physiol* 1984;14:C125–C142.
- Lovelock J. The denaturation of lipid-protein complexes as a cause of damage by freezing. *Proc Roy Soc London B* 1957;147:427–434.
- Mazur P. Slow-freezing injury in mammalian cells. In Elliott K, Whelan J, eds. *The Freezing of Mammalian Embryos*. Amsterdam: Elsevier;1977:19–42.
- Mazur P, Leibo SP, Chu EHY. A two-factor hypothesis of freezing injury. *Exp Cell Res* 1972;71:345–355.
- McGrath JJ. A microscope diffusion chamber for the determination of the equilibrium and non-equilibrium osmotic response of individual cells. *J Microsc* 1985;139:249–263.
- Gao DY, McGrath JJ, Tao J, et al. Membrane-transport properties of mammalian oocytes—a micropipette perfusion technique. *J Reprod Fertil* 1994;53:985–995.
- Gao DY, Benson CT, Liu C, et al. Development of a novel microperfusion chamber for determination of cell membrane transport properties. *Biophys J* 1996;71:443–450.
- Chen HH, Putteman JJP, Heimfeld S, et al. Development of a microfluidics device for determination of cell osmotic behavior and membrane transport properties. *Cryobiology* 2007;55:200–209.
- Devireddy RV, Swanlund, DJ, Roberts KP, et al. Subzero water permeability parameters of mouse spermatozoa in the presence of extracellular ice and cryoprotective agents. *Biol Reprod* 1999;61:764–775.
- Han X, Luo D, Cui X, et al. A modified differential scanning calorimetry method for determining water transport properties in biological cells during the freezing process. *Cell Preservation Technol* 2007;5:25–32.
- Angell CA. Supercooled water. *Annu Rev Phys Chem* 1983;34:593–630.
- Matsuoka S, Hibara A, Ueno M, et al. Supercooled micro flows and application for asymmetric synthesis. *Lab Chip* 2006;6:1236–1238.
- Lucke B, McCutcheon M. The living cell as an osmotic system and its permeability to water. *Physiol Rev* 1932;12:68–138.
- Mazur P. Equilibrium, quasi-equilibrium, and nonequilibrium freezing of mammalian embryos. *Cell Biophys* 1990;17:53–92.
- Leibo SP. Water permeability and its activation-energy of fertilized and unfertilized mouse ova. *J Membr Biol* 1980;3:179–188.
- Hunter JE, Bernard A, Fuller, BJ, et al. Measurements of the membrane water permeability ( $L_p$ ) and its temperature-dependency (activation energy) in human fresh and failed-to-fertilize oocytes and mouse oocyte. *Cryobiology* 1992;29:240–249.
- Jacobs, MH. The simultaneous measurement of cell permeability to water and to dissolved substances. *J Cell Compar Physiol* 1933;2:427–444.
- Kleinhans, FW. Membrane permeability modeling: Kedem-Katchalsky vs. a two-parameter formalism. *Cryobiology* 1998;4:271–289.
- Komatsu N, Kunitama M, Yamada M, et al. Establishment and characterization of the thrombopoietin-dependent megakaryocytic cell line, UT-7/TPO. *Blood* 1996;87:4552–4560.
- Gandhi MJ, Drachmana JG, Reems J, et al. A novel strategy for generating platelet-like fragments from megakaryocytic cell lines and human progenitor cells. *Blood Cells Mol Dis* 2005;35:70–73.
- Tatsuya K, Ryuji H, Hiroshi Y. The human megakaryocytic cell line UT-7/TPO expresses functional platelet agonist signals mediated through GPVI and thromboxane receptor. *Cell Biol Int* 2010;34:943–949.
- Hempling HG, Thompson S, Dupre A. Osmotic properties of human lymphocyte. *J Cell Physiol* 1977;93:293–302.
- Woods EJ, Liu J, Derrow CW, et al. Osmometric and permeability characteristics of human placental/umbilical cord blood CD34+ cells and their application to cryopreservation. *J Hematother Stem Cell Res* 2000;9:161–173.
- Green K, Downs S. Corneal membrane water permeability as a function of temperature. *Invest Ophthalmol* 1976;15:304–307.
- Noiles EE, Bailey JL, Storey BT. The temperature dependence in the hydraulic conductivity,  $L_p$ , of the mouse sperm plasma membrane shows a discontinuity between 4 and 0°C. *Cryobiology* 1995;32:220–238.

39. Crowe JH, Hoekstra FA, Crowe LM, et al. Lipid phase transitions measured in intact cells with Fourier transform infrared spectroscopy. *Cryobiology* 1989;26:76–84.
40. Eletr S, Inesi G. Phase changes in the lipid moieties of sarcoplasmic reticulum membranes induced by temperature and protein conformational changes. *Biochim Biophys Acta* 1972;290:178–185.
41. Quinn PJ. Lipid-phase separation model of low-temperature damage to biological membranes. *Cryobiology* 1985;22:128–146.
42. Drobnis EZ, Crowe LM, Berger T, et al. Cold shock damage is due to lipid phase transitions in cell membranes: a demonstration using sperm as a model. *J Exp Zool* 1993;265:432–437.

Address correspondence to:

*Mr. Hsiu-Yang Tseng  
Department of Mechanical Engineering  
University of Washington  
Seattle, WA 98195*

*E-mail: tsengh@u.washington.edu*

*Dr. Dayong Gao  
Department of Mechanical Engineering  
University of Washington  
Seattle, WA 98195*

*E-mail: dayong@u.washington.edu*

Received 14 June, 2011 / Accepted 4 August, 2011